3D PRINTED HIGHLY ELASTIC STRAIN SENSORS OF MULTIWALLED CARBON NANOTUBE/THERMOPLASTIC NANOCOMPOSITES

J. Christ, N. Aliheidari, A. Ameli[*]*, Advanced Composites Laboratory, School of Mechanical and Materials Engineering, Washington State University Tri-Cities, Richland, WA*
P. Pötschke, Department of Functional Nanocomposites and Blends, Leibniz Institute of Polymer Research, Dresden, Germany
[*] *Corresponding Author: Amir Ameli. Tel: 509-372-7442. Email: a.ameli@wsu.edu*

Abstract

3D-printable, flexible, and electrically conductive thermoplastic-based material was successfully developed for strain sensing applications. Thermoplastic polyurethane/ multiwalled carbon nanotube (TPU/MWCNT) nanocomposites were compounded, their filaments fabricated, and sensor samples 3D printed using fused deposition modeling (FDM). Mechanical, electrical, and piezoresistivity behaviors for bulk and 3D printed TPU/MWCNT nanocomposites were investigated under monotonous and cyclic loadings. The results revealed very modest decreases in the printed nanocomposites moduli (~14.4%, compared to those of bulk counterparts), indicating excellent interlayer adhesion and performance. Electrical conductivity was largely preserved after printing and piezoresistivity gauge factors for the printed and bulk samples were found to be similar, indicating no decay in the printed samples under applied strains as large as 100%. Furthermore, a highly repeatable resistance-strain response was observed under cyclic loadings. The results demonstrate TPU/MWCNT nanocomposites as excellent piezoresistive feedstock for 3D printing.

Introduction

Recently, significant research endeavors have been made in expanding the additive manufacturing (AM, *aka* 3D printing) technologies to a wide variety of applications [1–3]. The AM field employs a variety of manufacturing technologies. These technologies all function similarly in that they produce physical parts from a computer aided design (CAD) program by depositing the feedstock material, layer by layer, onto the build platform until the part is complete. Of primary interest within this research is Fused Deposition Modeling (FDM). In FDM process, the feedstock, typically a thermoplastic polymer, is fed into a heated nozzle where it is then extruded as a continuous bead of molten plastic. The nozzle is maneuvered by a computer numerical control machine which directs the path of the nozzle to pattern out the part as a series of discrete layers, building the part from the bottom, moving upward.

FDM 3D printing has seen significant publicity over the last decade. Due to the relatively simplistic mechanical design, affordability, and the capabilities of FDM machines, it has garnered significant interest in both industry and academia [4]. While the design of FDM printers has seen a rapid growth, the field of printable materials has also experienced a rapid influx of unique and novel thermoplastic materials; conductive, magnetic, flexible, and dissolvable filaments are just a few to name.

Conductive filler/polymer composites (CPCs) offer many functional uses within the strain sensing field, there has been significant research towards developing highly flexible sensors capable of measuring large strains as high as 400% [5]. This has been usually achieved by combining a highly flexible polymer with some type of highly conductive filler. Boland et al. [6] developed a high-strain motion sensor using a graphene-rubber nanocomposite for use as bodily motion sensing platforms. This was done by soaking rubber bands in a graphene solution. Morteza et al. [7] developed a flexible strain sensor by sandwiching silver nanowires within a polydimethylsiloxane (PDMS) polymeric matrix. They showed an accurate linear correlation between strain and resistance. In another work, Muth et al. [8] was able to fabricate strain sensors by embedding a carbon-based conductive ink within an elastomeric polymer using an inkjet printing process.

While these sensor designs have shown strong capabilities as strain sensing platforms, a facile fabrication method still remains as a common challenge for the current sensor designs. By developing a highly elastic, electrically conductive thermoplastic nanocomposite for FDM manufacturing, the fabrication of complex and multidirectional sensor patterns should be achievable without the need for complex processing methods.

This work focuses on developing a TPU/MWCNT based novel FDM feedstock that demonstrates high elasticity and excellent piezoresistive properties. Particular attention is paid towards the mechanical and electrical robustness of the FDM printed materials, compared to their bulk precursors. Moreover, the mechanical, electrical, and piezoresistive characteristics of the FDM printed TPU/MWCNT samples were investigated under both monotonous and cyclic loadings.

2. Experimental Procedure

2.1. Materials

TPU and MWCNT were used as the constituents of the nanocomposites. The TPU grade of Elastollan 1185A polyurethane supplied by BASF, with a density of 1.12 g/cm^3 and a shore hardness of 85A was used as the flexible matrix of the nanocomposites. NC7000 multiwalled carbon nanotubes of 90% purity having an average diameter of 9.5 nm and an average length of 1.5 μm were purchased from Nanocyl S.A., Sambreville, Belgium. Both materials were used as received. TPU and TPU/MWCNT were dried at 80°C for two hours before any melt processing.

2.2. Fabrication of TPU/MWCNT filaments

First, 5 wt. % MWCNT was dry blended with TPU and melt compounded to prepare TPU/5 wt. % MWCNT masterbatch. Extrusion was done using a Krauss Maffei Berstorff ZE 25, with a screw length-to-diameter L/D ratio of 36 where the melt temperature, and screw rotational speed were 221-229 °C, and 300 rpm, respectively. TPU was fed in the main hopper and carbon nanotubes were dosed into the side feeder attached at 14D.

For preparation of the TPU/MWCNT nanocomposites with diluted concentrations from the masterbatch, a 16 mm twin-screw extruder type LTE with L/D ratio of 16/40 (LabTech Engineering Company LTD., Thailand) was used. TPU/MWCNT nanocomposites with MWCNT content ranging from 1 to 5 wt. % were fabricated. At a given extrusion condition, the diameter of the extrudate varied as the MWCNT content was changed. The extrusion parameters were thus optimized such that a constant filament diameter could be obtained at various MWCNT contents while maintaining high level of shear loads. This was done by adjusting the 5 temperature zones and screw rotational speed. Melt temperature, and screw rotational speed were 180-210 °C, and 40-55 rpm, respectively. For the downstream collection and winding of the extruded filaments, a Filabot Spooler (Filabot, Vermont) was used.

FDM printing process requires highly consistent diameter of the filament. To assure the diameter consistency, the filaments were pelletized and re-extruded using a custom benchtop plunger extruder set to 200 °C with a nozzle diameter of 1.55 mm. The filament flow rate was set to 24.5 mm/sec. The resulting filament diameter was 1.55 mm ± 0.07 mm. These filaments were then used to FDM print the sensors and also to characterize the tensile, conductivity, and piezoresistive behaviors of the bulk nanocomposites.

2.3. Fused deposition modeling of TPU/MWCNT

The TPU/MWCNT filaments were FDM 3D printed using a MakerBot Replicator 2X Experimental Printer (MakerBot Industries, LLC, Brooklyn, New York). The FDM printing parameters were optimized for a better printability and are listed in Table 1.

It is noted that the same printing conditions were used for all the nanocomposites, having various MWCNT contents, so they can be directly compared. Samples for both stress- strain and resistance-strain tests were dimensioned at 1.6 mm ×1.6 mm with a length of 100 mm.

Table 1: FDM parameters used for the 3D printing of TPU/MWCNT nanocomposites

Parameter	***Value***
Print nozzle diameter (mm)	0.8
Nozzle temperature (ºC)	220
Bed temperature (ºC)	60
Layer height (mm)	0.2
Print infill (%)	100
Print Speed (mm/s)	20

2.4. Characterization

The static and cyclic tensile performance and piezoresistive behavior of the nanocomposite filaments and printed samples were characterized using a custom small-scale benchtop tensile loading machine. The loading rate for all the tests was set at 5 mm/s. In the case of cyclic loading, the load was applied to achieve the maximum strain, then the sample was unloaded to zero and held for 5 seconds, before the next loading cycle started.

For determining the percolation behavior of the bulk TPU/MWCNT nanocomposites, the extrudates was pelletized and pressed into disks of 14 mm in diameter and 3.17 mm in thickness. Pressing conditions of 200 °C and 2.25 metric tons for 10 seconds was applied using a 3851 Carver Hydraulic Laboratory Manual Press (Carver Inc., Wabash, Indiana). The disks' flat surfaces were then coated with CircuitWorks CW2400 conductive silver epoxy and the bulk electrical conductivity was obtained by measuring the resistance using a Fluke 8842A Multimeter.

The through-layer electrical conductivity of FDM 3D printed nanocomposites was measured on square samples with 10 mm sides and 3 mm thickness. To measure the cross-layer conductivity, 10 mm cubes were printed and then segmented into 3 mm thick slabs. The major flat surfaces were then coated in the silver epoxy and the conductivity was measured following the same method as for the pressed samples. This was done in order to determine if there is any loss in electrical conductivity and whether any anisotropic behavior is produced due to the FDM printing process.

3. Results and Discussion

3.1. Microstructure

To obtain enhanced and reliable electrical conductivity and mechanical strength in nanocomposites, it is very important to have a consistent dispersion of MWCNT within the TPU throughout the entire material matrix. Further, from the FDM printing requirements, it is critical that few to no MWCNT agglomerates are present within the TPU/MWCNT nanocomposites, as this can cause nozzle clogging and impede the printing process. Figure 1 shows a magnified view of an FDM 3D printed TPU/3 wt. % MWCNT sample with two layers in *y* direction. As Figure 4.a shows, a series of voids run down the center line indicating the points where two extruded layers meet. Within the extrudate layers, there are few to no inconsistencies indicating the good printability. As seen in Figure 4c-d, there are no major voids between the stacked layers along the *z*-axis indicating strong inter-layer adhesion.

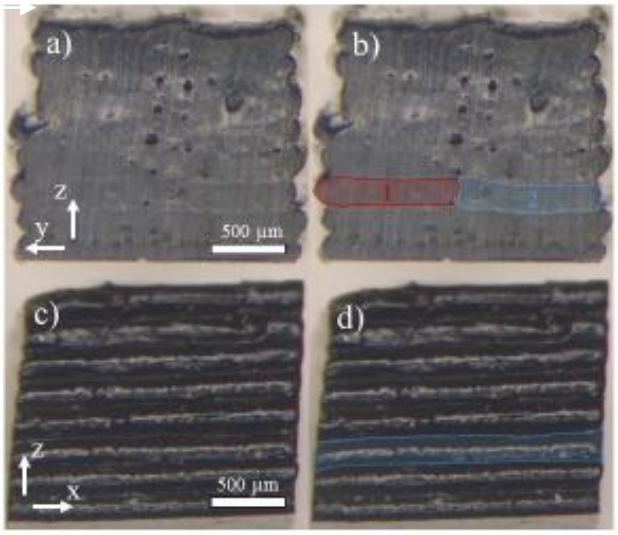

Figure 1: Structure of TPU/3 wt. % MWCNT a) cross-section; b) cross-section with highlighted extrudate layers in ***y***-direction; c) layer profile; d) profile with one highlighted extrudate layer. The layers were printed in the ***xy*** plane, stacked along ***z***-axis.

3.2. Mechanical properties

Figure 2 shows the stress-strain loading/unloading response of the extruded filament and the FDM 3D printed TPU/MWCNT nanocomposites. With the addition of MWCNTs, the strength of both extruded filament and FDM 3D printed nanocomposites increased. Overall, there is a slight decrease in the strength of the FDM 3D printed samples, as compared to their precursor filaments. This is inherent to the printing process leaving small interlayer voids and possibly interlayer imperfect bonding.

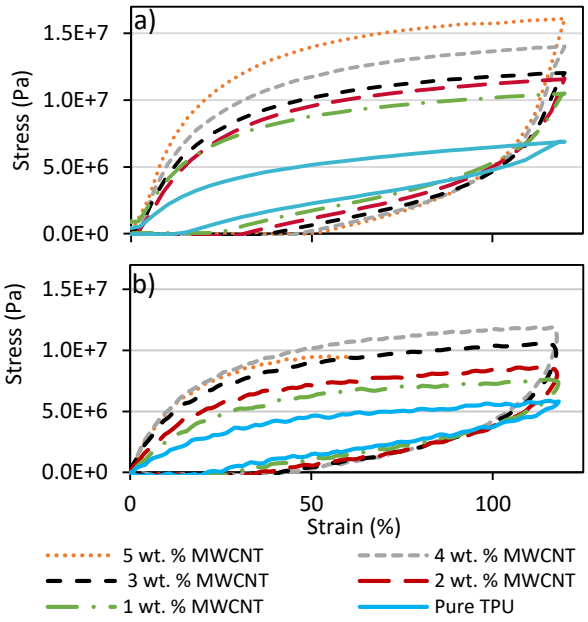

Figure 2: Stress-strain behavior of: a) extruded filament, b) FDM 3D printed TPU/MWCNT nanocomposites with various MWCNT contents loaded to 120% strain at 5 mm/s.

Figure 3 also compares the elastic moduli of the printed and the bulk filaments at different MWCNT contents. There is mild decrease in the modulus after printing. The average percent difference between the moduli of the filament and the corresponding printed samples is ~14.4%. This is markedly better than what has been demonstrated in the literature for printed ABS versus bulk ABS [9].

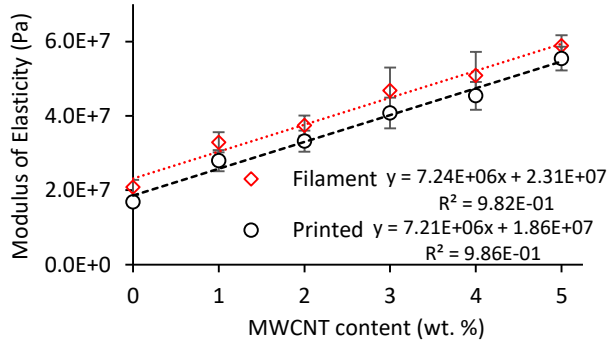

Figure 3: Modulus of elasticity obtained from the initial linear stress-strain response (Figure 2) of the filament and FDM 3D printed TPU/MWCNT nanocomposites

One desirable aspect to strain sensing materials is their ability to sense cyclic strains. Figure 4-a and Figure 4-b illustrate the cyclic behavior of FDM 3D printed pure TPU and TPU/4 wt. %MWCNT nanocomposite, respectively.

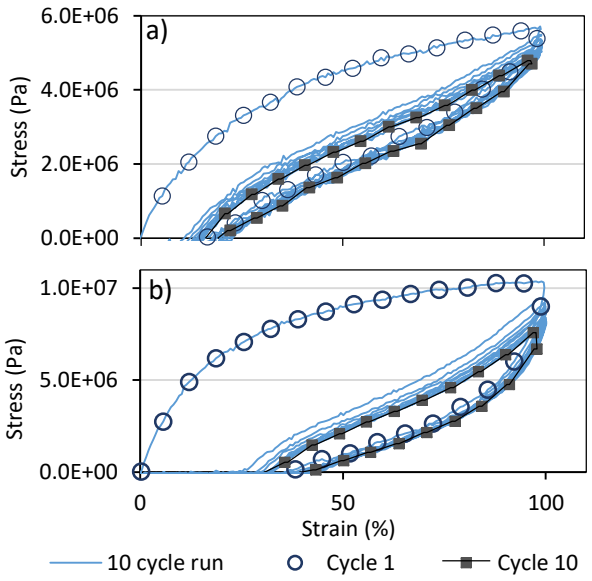

Figure 4: Stress-strain plots of FDM 3D printed (a) pure TPU and (b) TPU/4 wt. % MWCNT samples when loaded to a maximum strain of 100% for 10 cycles.

Both strain softening and the Mullins effect can be seen in the pure TPU as well as the TPU/MWCNT samples when cyclic strain is applied. This is a characteristic of elastomeric materials and their composites, as they tend to exhibit strain softening behavior when loaded cyclically [10]. The strain softening effect has been associated with the rearrangement of the polymer chains within the polymer matrix as well as a physical breakage of the polymer [11]. The Mullins effect can be described as the change in elastic behavior, often referred to as stress-softening, caused by initial strain loadings. In Figure 4a-b, the Mullins effect is evident by the overall decrease in maximum stress observed at the largest strain of 100%, as the cycle progresses. It is noted that both the strain-softening and Mullins effects are more pronounced in the case of nanocomposites, compared to the neat TPU.

3.3. Electrical Conductivity

Understanding the conductivity of composites as a function of filler loading has been well established within literature [12]. Figure 5 shows the through-layer and cross-layer conductivities of the FDM 3D printed samples as well as the through-plane conductivity of the pressed samples as a function of MWCNT content. Both through-layer and cross-layer conductivities of the FDM 3D printed samples demonstrated similar trends to that of the pressed samples with the conductivity values being in the same order of magnitude for a given MWNCT content. This indicated that the conductivity of TPU/MWCNT nanocomposites was preserved in both directions (through-layer and cross-layer) after FDM printing. It is also interesting to note that the printed samples exhibited slightly higher cross-layer conductivity at low MWCNT contents. The conductivity is strongly dependent on the MWCNT orientation [13]. It is possible that the printing process imparts some degree of orientation in the layer print direction, not found in the pressed samples, resulting in a better conductance in the cross-layer direction at lower contents where orientation has a greater effect.

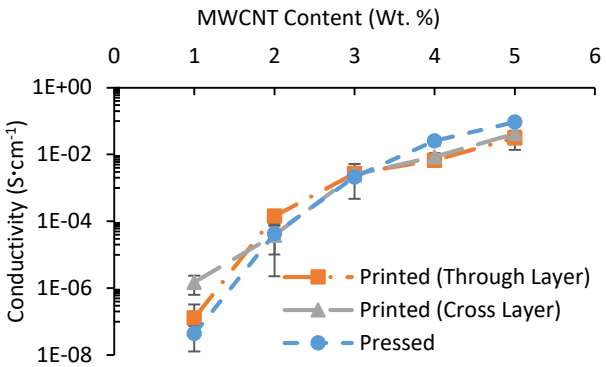

Figure 5: Electrical conductivity of the pressed and FDM 3D printed TPU/MWCNT nanocomposites as a function of MWCNT content

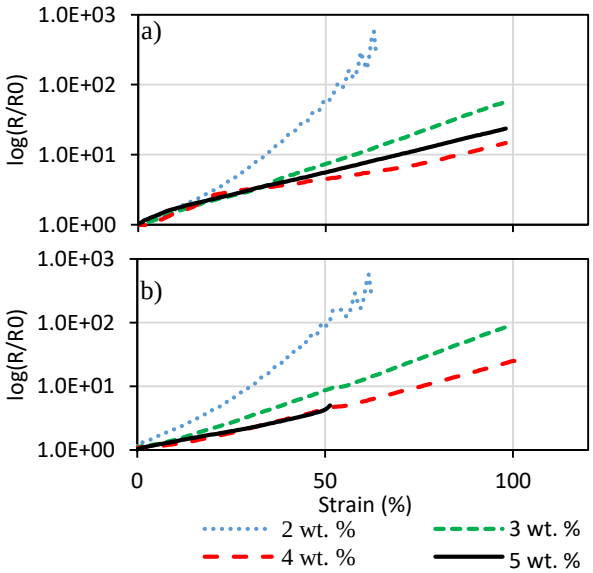

Figure 6: Logarithmic normalized resistance plots of: a) extruded filaments, and b) FDM 3D printed TPU/MWCNT nanocomposites as a function of strain during loading

The normalized resistance is defined as the measured resistance divided by the initial resistance and is widely used as a measure of sensor sensitivity, in the characterization of strain sensors. Figure 6a-b shows the normalized resistance log plots of the filaments and the FDM 3D printed samples, respectively, as a function of strain. It can be seen that as the MWCNT content varies, the normalized resistance response experiences a shift, where the response becomes more pronounced as the MWCNT content decreases. This aligns well with the percolation. This variable response to the MWCNT loading

provides a means of adjusting the response, and an effective strategy to tune the sensor sensitivity.

The gauge factor (GF) is often used as a means of quantifying the sensitivity of a strain sensing material. The GF is defined as,

$$GF = \frac{\frac{\Delta R}{R_0}}{\varepsilon} \quad (2)$$

where $\frac{\Delta R}{R_0}$ is the normalized resistance change and ε is the strain. Table 2 lists the gage factors for the FDM 3D printed and filament TPU/MWCNT samples. Except for the lowest MWCNT content (2 wt. %), the printed and filament samples demonstrated relatively similar gage factors.

Table 2: Gauge factors of the filament and FDM 3D printed TPU/MWCNT nanocomposites at 50% strain loading.

MWCNT	***2 wt. %***	***3 wt. %***	***4 wt. %***	***5 wt. %***
Filament	120.2	15.2	9.2	11.6
Printed	176.0	18.2	9.2	8.6

3.4. Cyclic Piezoresistive Behavior

In developing a sensor material, it is of significant importance to understand its behavior when placed under cyclic loading. Figure 7 shows a plot of the normalized resistance of the extruded filament and the FDM 3D printed TPU/3 wt. % MWCNT nanocomposite as a function of time with 100% strain applied for ten cycles.

Both the printed and extruded samples exhibited a very strong and consistent cyclic response with only a very slight decrease in performance over the cycle set. Further, the response curves showed nearly identical behaviors between the two types of samples, with the printed samples showing a slightly higher response spike at the maximum strain.

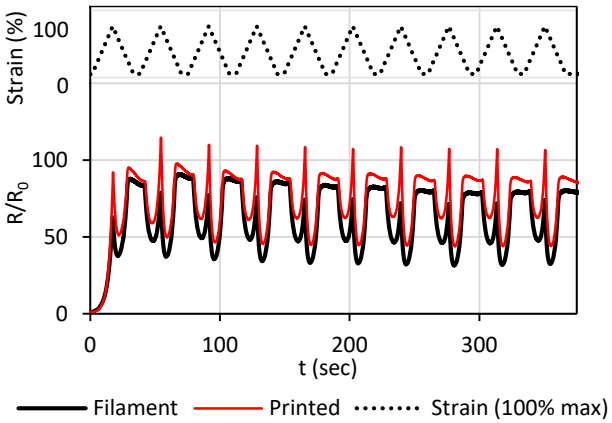

Figure 7: Cyclic strain plots of extruded and FDM 3D printed TPU/3 wt. % MWCNT samples over ten cycles at 100% strain loading

Of interest within the cyclic response is the non-monotonic behavior demonstrated by both sample types, as seen in Figure 7. Instead of a single-peak resistance characteristic, it demonstrated an inverse response to the strain load up until a certain strain (approximately 60%-70% strain here) where it then began to increase. Upon reaching the maximum strain, the resistance was maximized. The unloading pattern was found to be also similar to that of the loading phase. During unloading, the resistance decreased to a minimum value at a strain of ~ 50%, beyond which started to increase. This phenomenon is often attributed to the restructuring of percolation pathways creating a competition between the forming of new pathways and the destruction of old pathways [5]. The resistance decreases when the number of MWCNT interconnections increases. It is interesting to note that this behavior correlates well with its mechanical analog of the Mullins behavior (mechanical strength loss in Figure 4) in that there is a semi-permanent change in the strength of the sample caused by the strain at the first cycle. It seems that they both are governed by the strain softening within the first cycle which introduces some permanent deformation.

4. Conclusion

In this research, both extruded filaments and FDM 3D printed nanocomposites of TPU/MWCNT were created. Their mechanical, electrical, and piezoresistive behaviors were tested and compared. As is found in literature, with the increased addition of MWCNT filler, the material strength and initial elastic modulus was shown to increase. In order to obtain a fundamental understanding of materials' piezoresistive properties as a function of filler loading, the samples were subjected to various strain loadings and the electrical responses were measured and compared. From the results it was determined that, for the purposes of printing piezoresistive strain sensors, 3 wt. % loading of MWNCT offers sufficient sensitivity for the strains as high as 100%.

The cyclical response showed strong and consistent behavior over a range of strain loadings. Strain softening behavior was exhibited by the printed samples but showed consistency with bulk extruded material. Good printability was observed across all concentrations.

References

[1] Compton, B. G., and Lewis, J. A., 2014, Adv. Mater., **26**(34), pp. 5930–5935.

[2] Leigh, S. J., Bradley, R. J., Purssell, C. P., Billson, D. R., and Hutchins, D. A., 2012, PLoS One, **7**(11), p. e49365.

[3] Chizari, K., Daoud, M. A., Ravindran, A. R., and Therriault, D., 2016, Small, **12**(44), pp. 6076–6082.

[4] Lin, D., Nian, Q., Deng, B., Jin, S., Hu, Y., Wang,

W., and Cheng, G. J., 2014, ACS Nano, **8**(10), pp. 9710–9715.
[5] Flandin, L., Hiltner, A., and Baer, E., 2001, Polymer (Guildf)., **42**(2), pp. 827–838.
[6] Boland, C. S., Khan, U., Backes, C., O'Neill, A., McCauley, J., Duane, S., Shanker, R., Liu, Y., Jurewicz, I., Dalton, A. B., and Coleman, J. N., 2014, ACS Nano, **8**(9), pp. 8819–8830.
[7] Amjadi, M., Pichitpajongkit, A., Lee, S., Ryu, S., and Park, I., 2014, ACS Nano, **8**(5), pp. 5154–5163.
[8] Muth, J. T., Vogt, D. M., Truby, R. L., Mengüç, Y., Kolesky, D. B., Wood, R. J., and Lewis, J. A., 2014, Adv. Mater., **26**(36), pp. 6307–6312.
[9] Bellini, A., and Güçeri, S., 2003, Rapid Prototyp. J., **9**(4), pp. 252–264.
[10] Cantournet, S., Desmorat, R., and Besson, J., 2009, Int. J. Solids Struct., **46**(11–12), pp. 2255–2264.
[11] Qi, H. J., and Boyce, M. C., 2005, Mech. Mater., **37**(8), pp. 817–839.
[12] Bauhofer, W., and Kovacs, J. Z., 2009, Compos. Sci. Technol., **69**(10), pp. 1486–1498.
[13] Du, F., Fischer, J. E., and Winey, K. I., 2005, Phys. Rev. B, **72**(12), p. 121404.